EBSD Study of Indian Wootz Steel Artifacts to Infer Thermomechanical History by Observation of Carbide Distribution and Orientation

A. Sullivan* and M. Barnett
Centre for Material and Fibre Innovation, Deakin University, Geelong, Australia, 3217
* andrew.sullivan@deakin.edu.au

Introduction

Wootz is the name given to a crucible steel prepared in India. Coze [1] noted that the name "wootz" first appeared in printed form in a report by Pearson in 1795 [2]. However, the origin of the name itself is unclear though it was proposed by Yule and Burnell in the Hobson-Jobson Dictionary [3] that the word "wootz" could come from "ukku" in the Kanadda language.

The historical impact and subsequent fame of wootz weaponry in the ancient world has created interest in what has come to be seen as an advanced material even by modern standards [4]. Ancient wootz artifacts are classed as high carbon (hypereutectoid) crucible steels and are characterized by high strength, hardness, and wear resistance [5], but especially by their attractive surface pattern.

The ingots used to make wootz implements known to have been cast from as early as 300 BC, continuing into the 1700s, at which time the casting and forging knowledge declined and was eventually lost. No detailed written records exist of the forging methods used to make weapons and implements from cast wootz ingots [6], leading to numerous duplication methods. Recent attempts have ranged from good approximations to almost identical reproductions [7–10]. Notably absent from historical accounts are details of forging temperature, cooling rates, and the strains imparted at each forging step. This has prevented modern attempts to "rediscover" the ancient blacksmiths' method in which hot shortness during forging and duplication of the surface pattern are known obstacles.

Hot shortness causes the ingot to crack during forming and results from softening and melting of the pro-eutectoid cementite on prior austenite grain boundaries while working at white heat. This problem has largely been solved by forging at temperatures slightly above the A_1 temperature (say ~750°C), thus enabling controlled breakage and spherodisation of the proeutectoid cementite (see Figure 1).

Duplication of the surface pattern has been more difficult and the mechanism by which it forms has been contested by a number of researchers [7, 8, 11–14]. The materials and methods used to produce and forge wootz ingots directly affect whether or not a pattern can be produced. It is generally agreed that for artifacts having hypereutectoid compositions, the surface pattern results from a banded distribution of proeutectoid carbides alongside eutectoid carbides in a ferrite matrix formed during multiple forging cycles.

Other studies have shown the importance of characterizing the various carbide forms because they are useful in determining deformation and metallurgical history [15, 11, 16]. The extent and pattern of deformation is indicated by banding, cracking, and crystal orientation in the coarser, blocky type cementite [17]. Metallurgical changes during forging are indicated by the morphology and crystal orientation of grain boundary (Widmanstatten and/or proeutectoid) and fine spheroidal cementite (spherodized pearlite and/or divorced eutectic) [13, 18, 17].

Two notable theories have been forwarded by Sherby and Wadsworth and by Verhoeven and Pendray to explain the origin of the proeutectoid carbides in forged wootz steel artifacts. Sherby and Wadsworth used a method of thermomechanical treatment employing hot and warm rolling to process pieces of hypereutectoid steels within a narrow temperature range [8]. Such tightly controlled temperature during processing means their experiments are precise and reproducible, but the applicability of the work to genuine wootz microstructures has been questioned [14]. The microstructures resulting from this method contain carbide patterns similar to ancient artifacts made from crucible steel, but there are notable differences. One

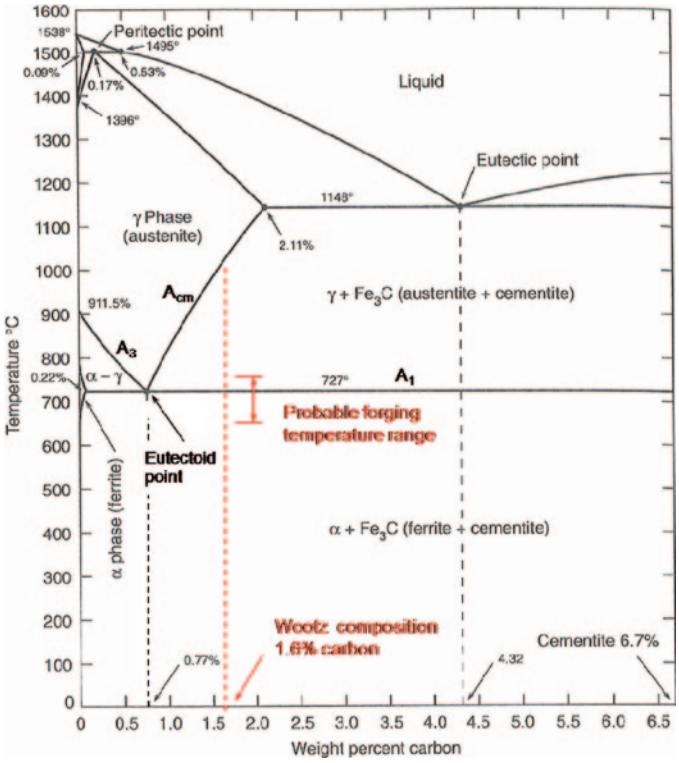

Figure 1: The iron-carbon phase diagram showing Wootz as a hypereutectoid steel with carbon content 1.6%, forged from cast ingot at high temperature using multiple cycles.

significant difference is that all of the visible banding is in line with the direction in which the steel was rolled. Wadsworth and Sherby claim that this is simply an artifact of the production method, but no further processing has been carried out to prove their method could produce the appropriate banding if it were forged [19]. Verhoeven and Pendray proposed that the formation of the pattern is due to the alignment of spherodised cementite in the interdendritic zones where impurities accumulate during solidification. They determined that elements such as vanadium and molybdenum, even in quantities as low as 0.003 percent, promote the alignment of cementite at interdendritic zones through a selective ripening process [11]. Other elements, which also promote banding, are chromium, niobium, and manganese [7]. Furthermore they showed that the banding behavior disappears and reappears with repeated thermal cycling [13].

Debate over the origin and development of coarse carbide bands in wootz steel continues, and new methods of analysis offer alternative ways of interpreting these complex microstructures. Where previous work has relied mainly on light microscopy to learn about the metallurgical structures involved, the use of electron back scatter diffraction (EBSD) in the study of wootz steel is a new method in this field, with recent precedents in work done by Barnett and Balasubramaniam [15, 18]. Unlike light microscopy investigations that can inspect artifact surfaces in their as-received condition, EBSD is destructive because the surface being analyzed must be finely polished. The advantage of data obtained by EBSD is that it contains unique information about the alignment of the crystal lattice, including metal grain and precipitate orientations and also phase distributions.

This study uses EBSD to investigate and identify relationships between carbide microstructure and thermomechanical history by collecting Euler angle data from crystal unit cells in polished wootz steel sections.

Compared to the more famous Damascus weaponry, traditional Indian weapons and implements made from wootz steel are less studied. This research summary presents an EBSD characterization of three Telangana artifacts from southern India, as identified in Table 1; two swords and one toddy tapper tool.

Electron Backscatter Diffraction (EBSD)

When an electron beam is incident on a tilted crystalline sample, electron backscatter diffraction patterns are generated through an interaction with a small volume of the material (~20–50 nm in diameter) (see Figure 2a). In the present studies, EBSD data were collected on a Leo 1530 field-emission SEM, using an HKL Nordlys detector.

Table 1: Wootz artifact descriptions. Note that all items are hypereutectoid steels.

Artifact	Place of Origin	Carbon Content*	Function
Blade 1	Northern Telangana (Konapuram)	1.6%	Weapon
Blade 2		1.6%	Weapon
Toddy tapper		1.84%	Plant cutting

* Glow discharge optical spectrometry

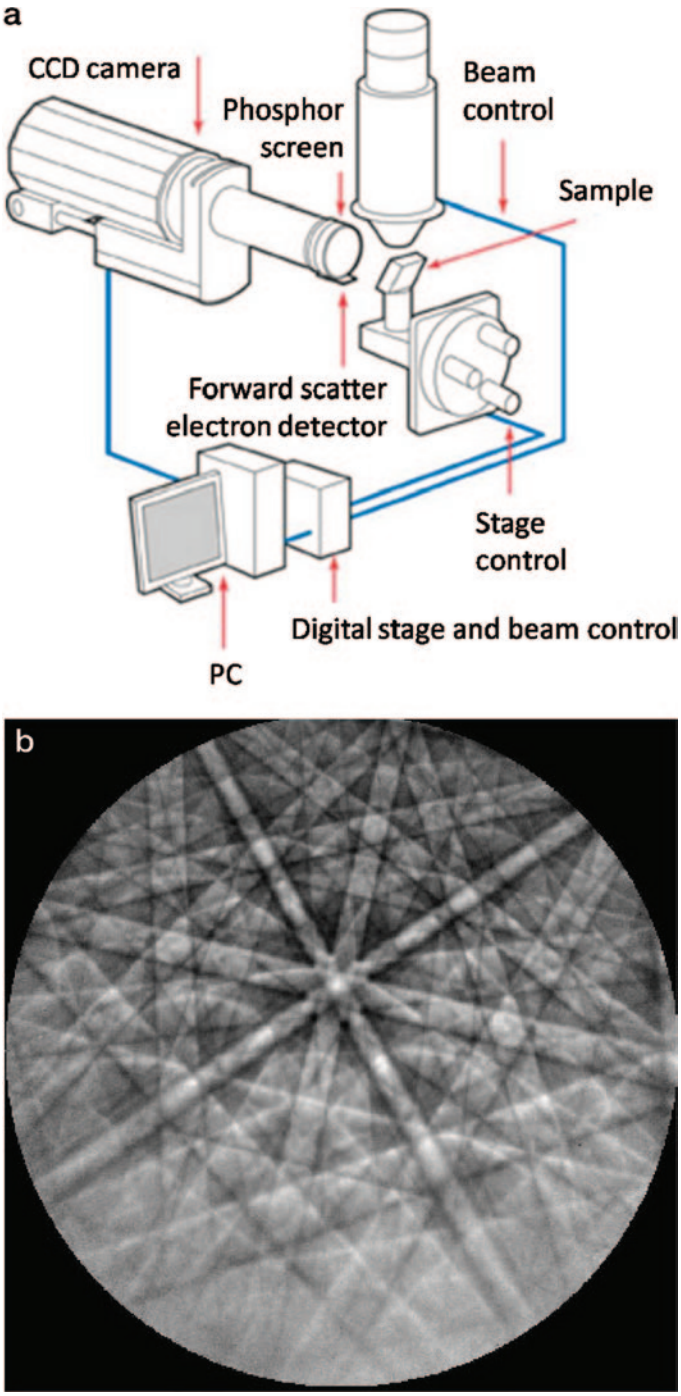

Figure 2: (a) Electron Backscatter Diffraction (EBSD) system schematic, (b) Kikuchi pattern [20].

The mechanism by which the diffraction patterns are formed can be described by the following principal features. The atoms in the material inelastically scatter a fraction of the electrons with only a small loss of energy to form a divergent source of electrons close to the surface of the sample. Some of these electrons are incident on atomic planes at angles that satisfy the Bragg equation ($n\lambda = 2d \sin\theta$), where n is an integer, λ is the wavelength of the electrons, d is the spacing of the diffracting plane, and θ is the angle of incidence of the electrons on the diffracting plane. These electrons are diffracted to form

Quemesa
2009

MegaView G2
KeenView G2
2008

Cantega G2
2007

Veleta
2006

Morada
2004

MegaView III
2001

KeenView
2000

MegaView II
1999

MegaView I
1997

ADDA
1989

OLYMPUS
Your Vision, Our Future

Quemesa

11 Megapixel High Speed TEM Camera

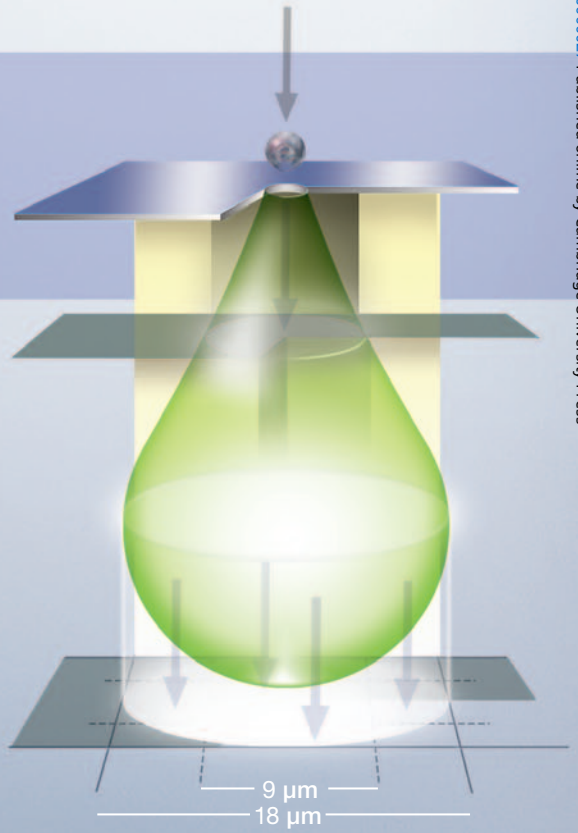

Obtaining the best possible photon yield in the scintillator per incident electron is done by matching the pixel size to the interaction volume through optimization of scintillator thickness.

EVERYTHING COUNTS

High sensitivity and contrast at optimal resolution are the ultimate goals for each TEM camera. Every single photon generated in the scintillator per incident electron is needed. This means the scintillator has to be optimized for the entire pear-shaped interaction volume to achieve maximum signal.

Consider the Quemesa, the new 11 Megapixel, on-axis TEM camera by Olympus Soft Imaging Solutions, where scintillator thickness and pixel size are perfectly matched to the dimensions of the entire interaction volume. This ensures the maximum number of photons is detected and guarantees an outstanding output signal from the cooled CCD chip: the essential requirement for high sensitivity and excellent contrast.

But Quemesa offers so much more: a visual field the size of a photo plate and high frame rates enabling real live-image work on your monitor.

Because, everything counts.

That's what Quemesa stands for – superior technical implementation and optimal user friendliness.

www.soft-imaging.net
info.osis@olympus-sis.com

North America: (888) FIND SIS, +1 (303) 234-9270
Europe: +49 (251) 79800-0
Asia / Pacific: +65 67777898

ELECTRON MICROSCOPY
MADE SIMPLE – SINCE 1986

North America | Europe | Asia | Pacific

OLYMPUS SOFT IMAGING SOLUTIONS

https://doi.org/10.1017/S1551929510000027 Published online by Cambridge University Press

a set of paired large-angle cones (Kossel cones) corresponding to each diffracting plane. When used to form an image on the fluorescent screen, the regions of enhanced electron intensity between the cones produce the characteristic Kikuchi bands of the electron backscatter diffraction pattern (see Figure 2b).

The center line of each Kikuchi band corresponds to the intersection with the phosphor screen of the diffracting plane responsible for the band. The Kikuchi bands as a group are characteristic of the single crystal's structure and orientation. The angular position of the Kikuchi bands can be found automatically with a Hough transform [20] and used in conjunction with a crystallographic database to calculate the crystal orientation of the sample region that formed the pattern.

The measured crystal orientations are displayed in Euler angle maps and in pole figures. Euler angles are used to describe crystallite orientations within a specimen. This involves specific rotations that transform the sample coordinate system into the crystal coordinate system and vice versa. The Bunge convention [21] is most commonly used in metallurgy (see Figure 3).

Pole figures are stereographic projections for chosen crystal directions. An example of a pole figure construction for a simple cubic crystal is shown in Figure 4. When a single grain is orientated in a particular manner relative to the specimen, the <100> normals to the cube planes project onto a sphere as shown in Figure 4a. A plane parallel to the specimen surface and passing through the center of the sphere intersects the sphere as a circle. The points where the <100> normals touch the sphere are then joined to the sphere's opposite pole (South Pole for points in the upper hemisphere. The stereographic projection (pole figure) is the shaded equatorial plane containing the poles 1′, 2′, and 3′ in Figure 4a. This process converts three-dimensional crystallographic directions into a set of two-dimensional points (Figure 4b). Only the upper hemisphere points are shown. This is repeated for the orientations of other grains in the sample to produce a pole figure that shows the distribution of that particular set of planes. If there is a tendency for the points to be arranged in a particular manner then this is called a *texture*. Furthermore, these data points are usually contoured to reflect the density or strength of any textures that may be present. The mean uniform density or MUD value in a pole figure shows the strength of the clustering of data relative to that from a random distribution.

All EBSD data presented in this article have undergone a two-step noise reduction procedure to clean the maps at pixels where no or very poor quality EBSD patterns are generated because of grain boundaries, cracks, dislocation clusters, voids, inclusions, or around regions of damage on the sample surface. The first step of noise reduction involves the replacement of pixels having an orientation different from

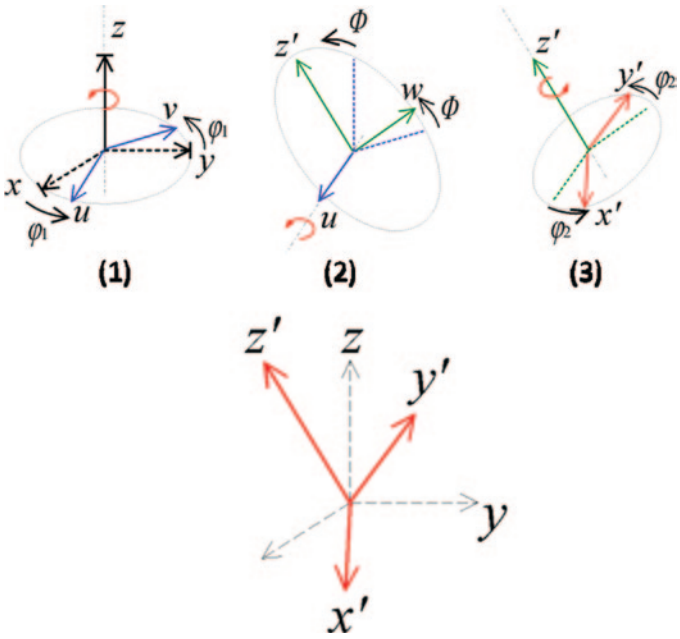

Figure 3: The three Euler angles: (φ_1, Φ, φ_2) represent the following (ordered) set of rotations, which are defined here. (1) A rotation of φ_1 about the *z*-axis followed by, (2) a rotation of Φ about the rotated *x*-axis (*u*) followed by, (3) a rotation of φ_2 about the rotated *z*-axis (*z*′).

all neighbors ("lonelies") with Euler angles of the dominant surrounding orientation. The second step involves filling non-indexed pixels (zero solutions) with Euler angles that are interpolations of the neighboring pixels. This has been applied in stages beginning with eight-neighbor pixels (conservative) and progressively decreasing the number of neighbors to one, until no un-indexed pixels remain in the map. Noise reduction has been applied equally to both the ferrite and cementite phases. Noise reduction is performed on the Euler data so that sub-grain orientation gradients are more readily observed in the cementite. Pole figures are relatively unaffected by this process.

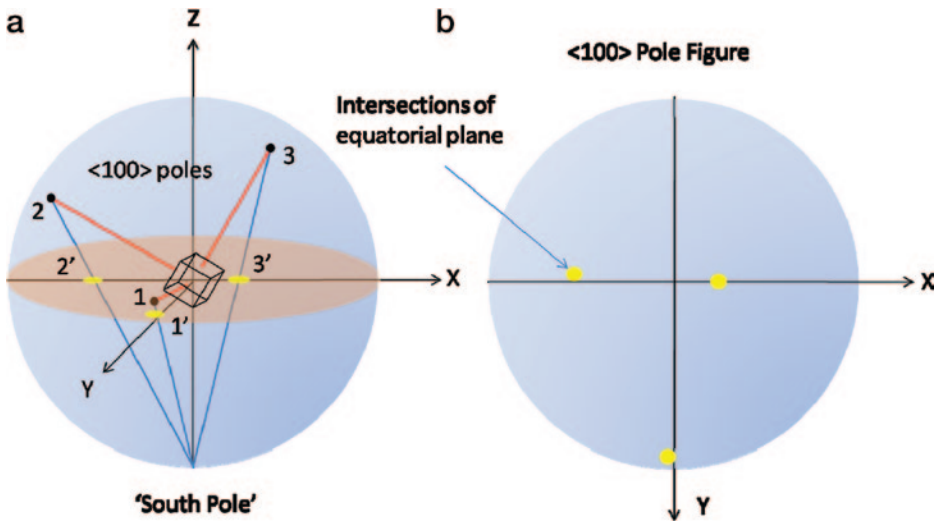

Figure 4: (a) <100> pole figure construction depicting the cubic unit cell at an arbitrary orientation relative to the sample. The sample surface is parallel to the equatorial plane. (b) The resulting pole figure (stereographic projection of the poles 1, 2, and 3).

Results

Three different Indian artifacts were analyzed by EBSD to characterize the carbide population. Sampling locations are identified in Figure 5. Carbide breakage is evident as voids in the microstructure that produce no data, and crystallographic alignment is displayed in pole figures. Low-angle boundaries within individual carbide particles are displayed as an overlay on low-magnification Euler angle maps of the carbide phase. Breakage and rotation are indicated by orientation clustering and rotation. Crystallographic orientation, spatial distribution, and/or ripening are displayed in high-magnification Euler angle maps of the fine carbide phase. This study presents orientation clustering data for coarse and fine carbides for each wootz artifact.

Two types of orientation clustering of the carbides were observed in the swords and to a lesser extent in the toddy tapper tool: (a) a micron-scale clustering within the *coarse* carbide bands with band spacing ranging from 30–100 μm and (b) a *fine* micron to sub-micron scale clustering of spheroidal particles, closely associated with proeutectoid cementite lying along prior austenite grain boundaries.

It is proposed that coarse carbide bands and fine carbide dispersions retain useful information about the forging method used to manufacture wootz artifacts. The proposed forging direction is indicated by carbide breakage and crystallographic alignment in the coarse carbide population. The impact of forging strain on the microstructure is indicated by the presence of low Euler angle boundaries and by the extent of breakage and rotation of coarse carbide particles. Forging temperature effects are indicated by the crystallographic orientation, spatial distribution, and/or ripening of fine carbides.

Coarse Carbide. Orientation clustering behavior in the carbide particles is detected by inspecting EBSD maps set to display Euler angles on a color scale. For each case, particles having the same or similar Euler angle color are identified as a group. Within each group of particles a single fragment is selected as a reference, approximately near the center of the cluster (in orientation space), and a gray scale assigned ranging from black to white, where black represents the reference orientation and white represents a deviation of 20° (Figure 6c, Figure 7c, Figure 8c). Although a 20° deviation of Euler angle was chosen arbitrarily, it is based on the assumption that if fragmentation of a single carbide particle occurs, the resulting fragments will rotate away from the starting orientation as the particles are worked into bands. The amount of rotation is expected to be proportional to the amount of strain imparted during forging. The objective is to test the concept that carbide banding is at least in part the result of fragmentation and subsequent alignment of as-cast coarse carbides in response to forging hammer blows. Forging impacts are known to be repeatedly applied to a cylindrical casting in order to produce a blade, thus forcing carbides to break and move by a combination of translation and rotation into sheets within the ferrite matrix.

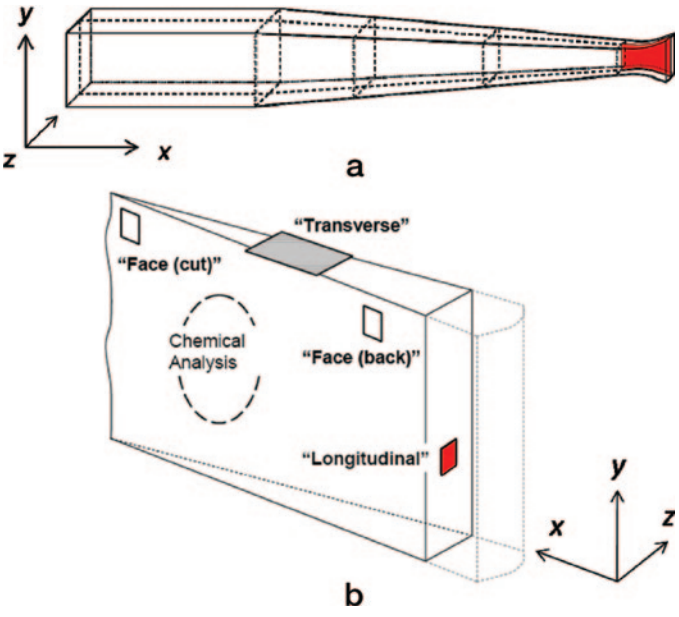

Figure 5: EBSD mapping regions indicated in red on the schematics for each artifact: (a) toddy tapper and (b) blades 1 and 2 with *z* ‖ [010] axis. The dotted lines in (b) show where inhomogeneous material was removed prior to analysis.

The sword blades investigated here both contain carbide bands that display particle clusters having similar crystallographic orientations. This can be seen on a large scale by viewing the color groupings in a Euler angle map in which the clusters are spread in bands on the long axis of the blade, thereby forming the characteristic long-range carbide bands of warm-worked wootz microstructures (Figure 6a and Figure 7a). These bands regularly intersect the blade surface at shallow angles and are thought to be the origin of the well-known patterning. The orientation clustering behavior is highlighted by examining a subset of a typical carbide cluster (Figures 6b and 6c, Figures 7b and 7c). The other artifact is a tool with a different use and a different microstructure (Figure 8a). The carbide banding in this tool has a significantly weaker texture than the sword blades, as shown by the low mean uniform density value (MUD) in a [010] pole figure. The weaker texture is assumed to be in part due to the lower forging reduction and possibly due to higher temperature forging; however, orientation clustering is still visible.

In addition to orientation clustering characterization, bulk texture data from the carbides were analyzed and used to confirm the predominant deformation direction during forging. Although this direction is known to be edge-wise hammering for the wootz ingot used to fabricate the swords (Figures 9a and 9b), the forming direction for the toddy tapper is not known (Figure 9c). Orthorhombic cube [010] textures were observed in all three artifacts parallel to the hammering direction during forging. Swords 1 and 2 measured high MUD values, 12.3 and 14.3 respectively (Figures 6d and Figure 7d). The toddy tapper displayed a significantly weaker [010] texture of 4.5 (Figure 8d). However, it is sufficient to infer that the principle-forging axis is on the axis shown in Figure 10. The tapper is likely to have experienced two directions of forging, and this has apparently weakened the texture.

In addition to the carbide orientations, the ferrite matrix was also analyzed for evidence of texture. The bulk texture of the ferrite is shown in terms of {001}, {110}, and {111} pole figures in Figure 11. The texture is weak. No significant difference is evident in the texture of the blade face or cross section. No systematic local grouping of orientations of ferrite was apparent.

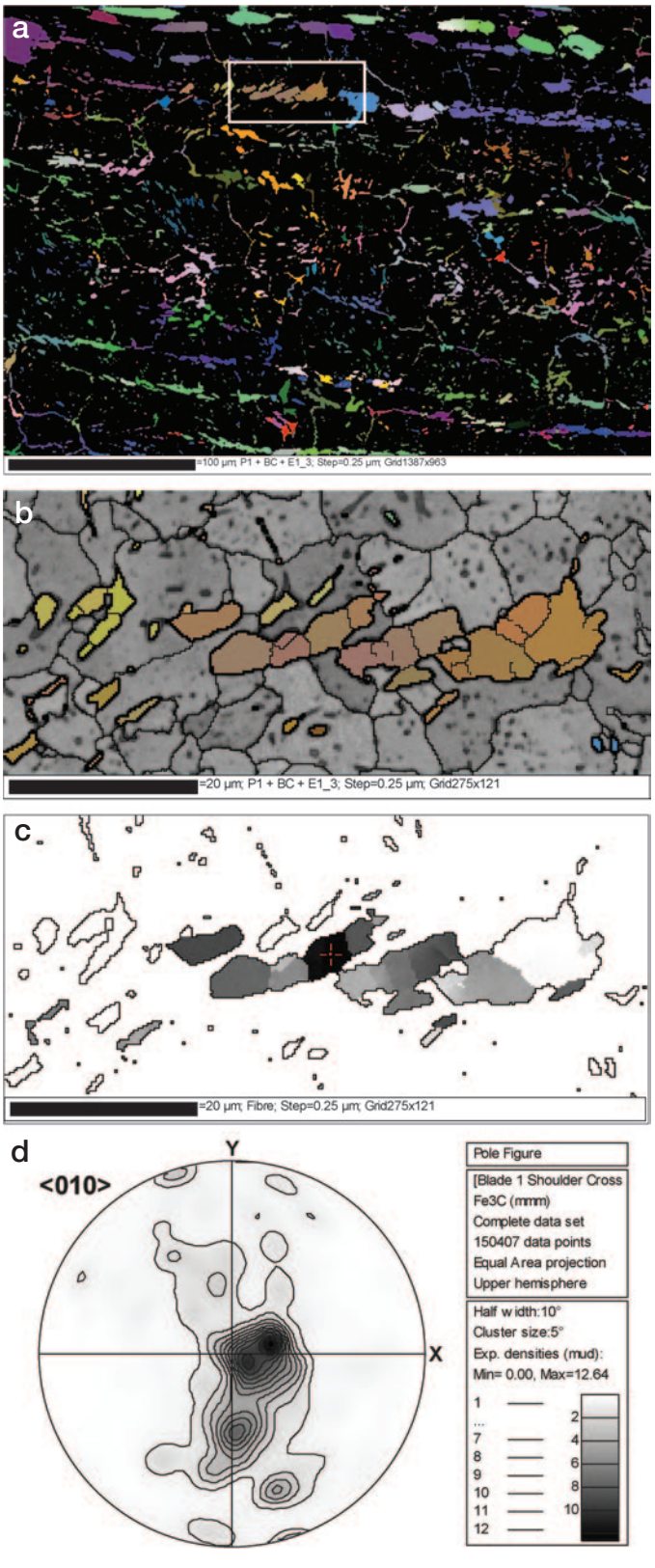

Figure 6: Sword 1 EBSD data. (a) Large area map showing carbide banding and crystal orientation, (b) pattern quality inset map showing cementite orientations among ferrite grains, (c) cementite orientations within 20° of the orientation of a reference particle within the group. Suggested forging direction is vertical in all images. (Black = selected orientation, white = greater than 20° misorientation). (d) Long-range texture of the carbide phase based on 347 × 241 µm mapping area.

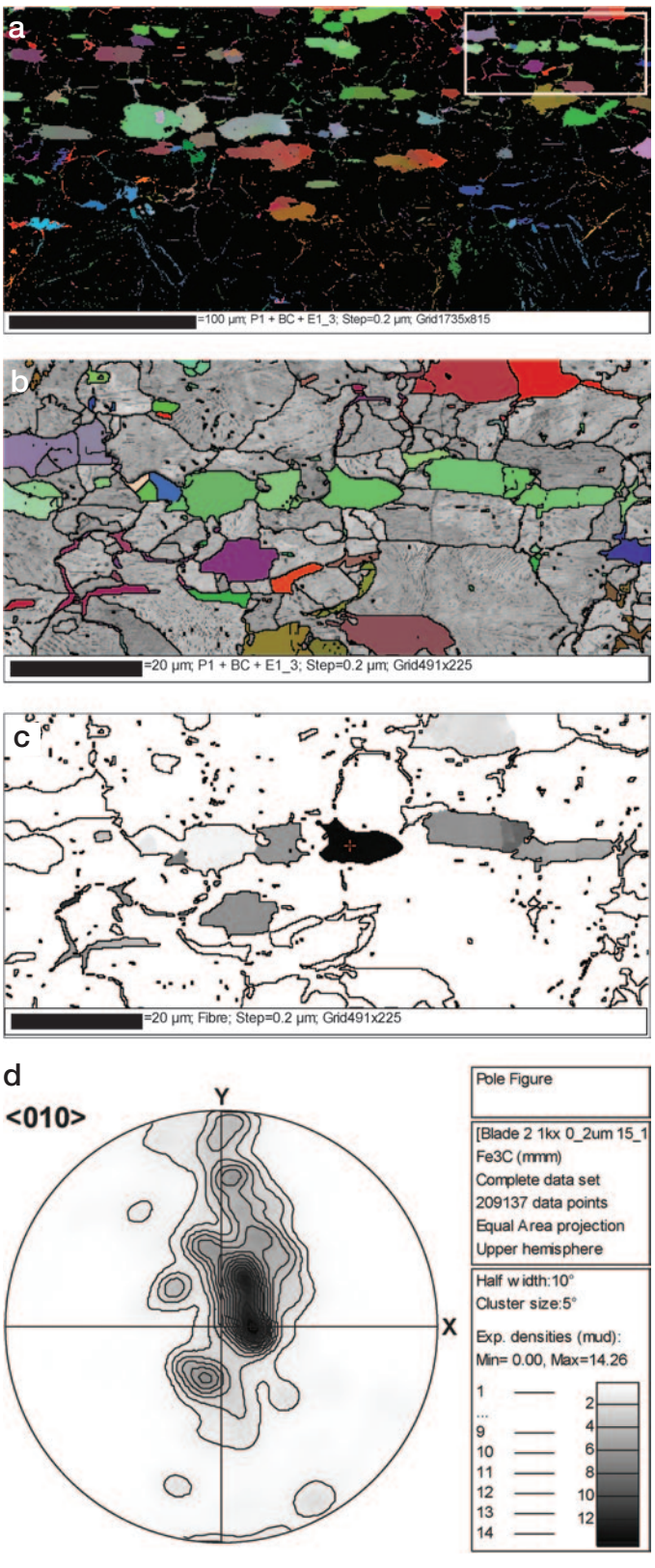

Figure 7: Sword 2 EBSD map. (a) Large area map showing carbide banding and crystal orientation, (b) pattern quality inset map showing cementite orientations among ferrite grains, (c) cementite orientations within 20° of the orientation of a reference particle within the group. Suggested forging direction is vertical in all images. (Black = selected orientation, white = greater than 20° misorientation). (d) Long-range texture of the carbide phase, based on 347 × 259 µm mapping area.

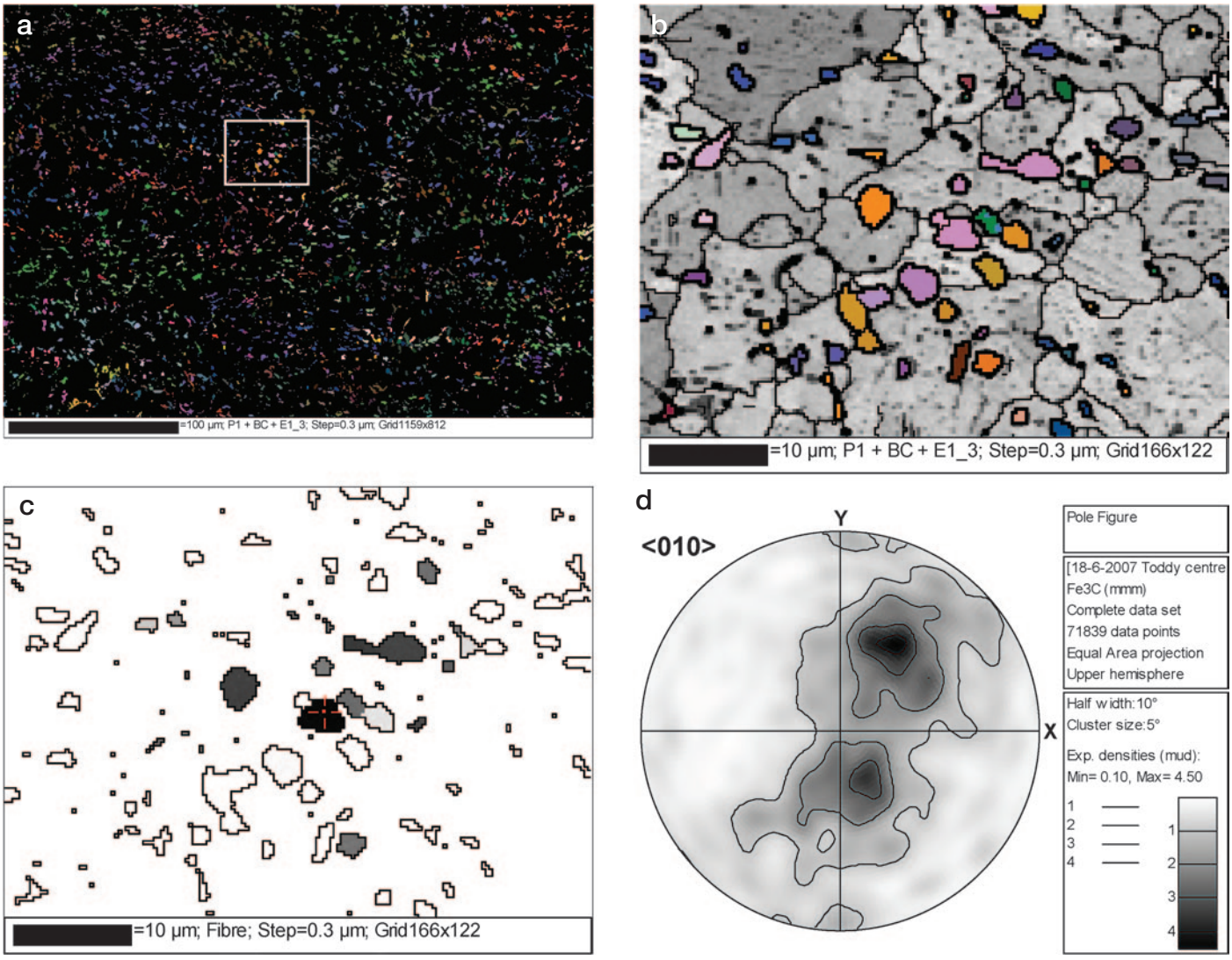

Figure 8: Toddy tapper EBSD map. (a) Large area map showing weak carbide banding and crystal orientation, (b) pattern quality inset map showing cementite orientations among ferrite grains, (c) cementite orientations within 20° of the orientation of a reference particle within the group. Suggested forging direction is predominantly vertical in all images, with some in the *z*-axis (out of the page). (Black = selected orientation, white = greater than 20° misorientation). (d) Long-range texture of the carbide phase based on 348 × 244 µm mapping area.

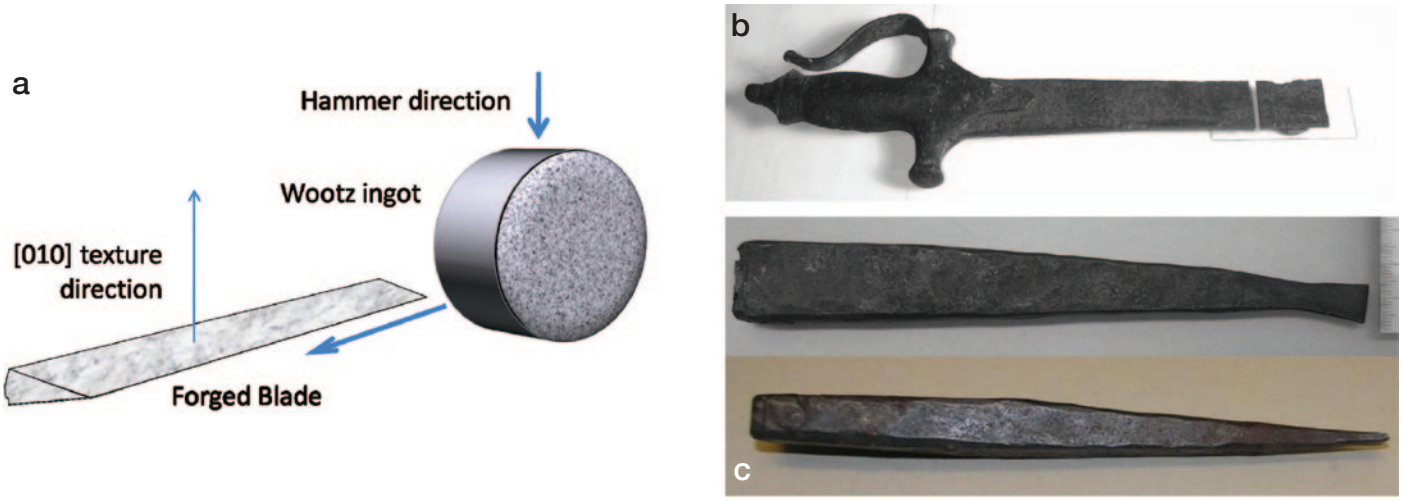

Figure 9: Texture indicates predominant deformation direction as shown: (a) for swords, (b) sword blade 1, and (c) the toddy tapper tool (side and top views).

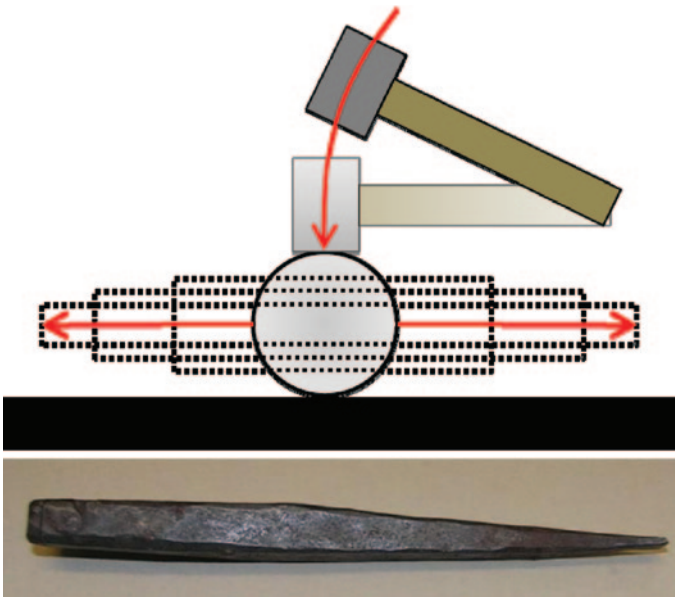

Figure 10: Predominant toddy tapper forming axis based on texture data.

The data from the two sword blades strongly support the hypothesis that the clusters of coarse carbides with similar orientations originate from a single proeutectoid cementite plate or crystal that has remained undissolved since casting and fragmented during forging cycles. The toddy tapper implement, while weaker in habit, demonstrates the same principle.

Fine Carbide. Investigation of the three artifacts found clusters of a fine submicron dispersion of cementite with an orientation relationship to neighboring pro-eutectoid cementite on prior austenite grain boundaries (Figure 12). This clustering phenomenon differs from that found in the coarse carbides in that no evidence of fragmentation or rotation can be associated with the orientation grouping. Coupled with the spheroidal nature of these carbides, this suggests that they contain information about the heat treatment cycle used to manufacture the artifacts. The observed crystallographic orientation distribution is consistent with either (1) formation from pearlite by spherodising of pearlite lamellae or (2) by the divorced eutectoid transformation (DET) [22], or a combination of both mechanisms as local microstructural variations dictate.

Whichever type of nucleation is occurring, the fine particles are adopting the same crystal orientation as the carbide along the prior austenite grain boundaries. The mechanism by which this can occur is not certain because it is clear that both pearlite and divorced eutectoid are present at different locations in the microstructure, depending on the austenising temperature and the weight percent of carbon. Both of these factors can vary significantly throughout the material because the thickness of the artifact and therefore the rate of heat loss during cooling changes from the cutting edge to the shoulder of the sword (~0.1–3 mm). The thickness variation is even more pronounced in the toddy tapper (~2–20 mm).

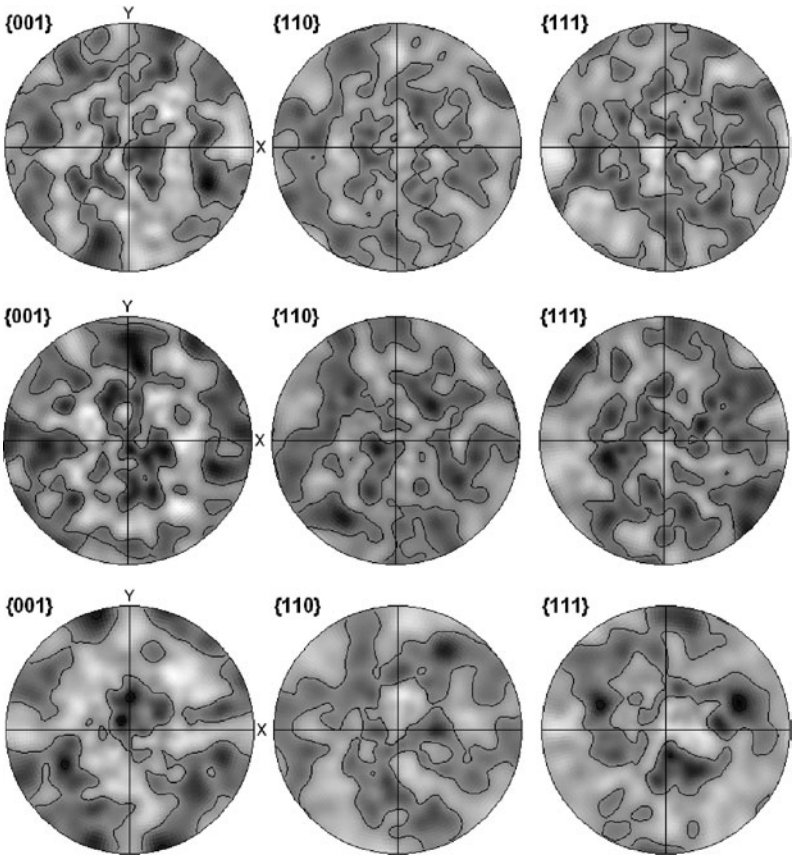

Figure 11: Crystallographic textures of the ferrite matrix for the same sample area as the carbide analysis for (a) toddy tapper, (b) blade 1, and (c) blade 2. Suggested forging direction is along the *Y*-axis in all pole figures.

If the fine particles originate from pearlite, then the orientation grouping can be explained by considering that the pearlite has grown from the cementite according to the Baryatski relation [23]. If the fine particles are forming by the DET mechanism, then their orientation grouping is previously unexplained. Pearlite spherodisation is well documented in steels, whereas the non-bainitic DET reaction is not, though this type of DET transformation is known to be favored by annealing at no more than 50°C below the A1 in the iron-carbon phase system (Figure 1), which is consistent with experiments by Verhoeven and Gibson [22].

A possible explanation for the orientation grouping in this case is that the pearlite is in fact forming at the early stages of forging but undergoes incomplete dissolution on successive reheats such that viable cementite nuclei remain in the microstructure at spacings typically associated with DET (~0.2 μm).

Conclusions

Two types of carbide orientation clustering have been observed in three wootz artifacts. Coarse carbides display an orientation clustering behavior where zones of similar orientation (measured within a 20° spread) occur in bands that are formed during forging. This suggests an as-cast particle origin. It is suggested that this provides a means of probing the forging history. Furthermore, a [010] texture was observed in the carbides, and a random texture was

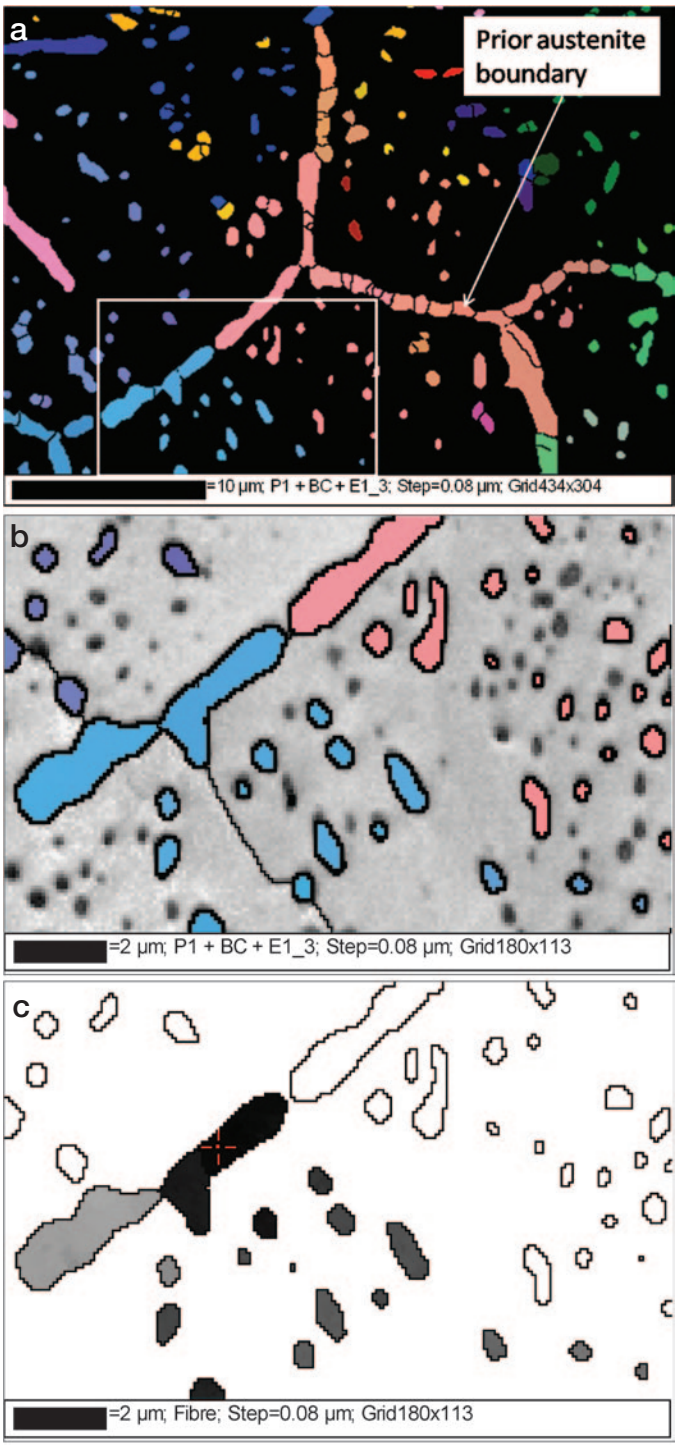

Figure 12: Blade 1 fine carbide (a) large area map showing fine carbide crystal orientation clustering and their relationship to prior austenite grain boundaries, (b) pattern quality inset map showing cementite orientations, (c) cementite orientations within 20° of the orientation of a reference particle within the group. (Black = selected orientation, white = greater than 20° misorientation).

observed in the parent ferrite grains for each artifact, confirming the direction of hammer blows used to forge the items. Although this was known in the swords, it was previously not known for the toddy tapper.

Fine carbides were observed to have an orientation clustering habit in close proximity to prior austenite grain boundaries. Although their origin is unclear, these particles are submicron and therefore more likely to dissolve during forging, thus providing information about the temperature history of the material, in particular the distribution of cementite within the ferrite at the onset of the final cooling cycle [24].

References

[1] JL Coze, *Journal of History of Science*, 38(2) (2003) 117–127.
[2] G Pearson, G., *Phil. Trans. Roy. Soc*, 85(A) (1795) 322–346.
[3] H Yule and Burnell, *Hobson-Jobson, the Anglo-Indian Dictionary*. 1st Edition, ed. 1886.
[4] S Srinivasan and S Ranganathan. *Wootz Steel: An Advanced Material of the Ancient World*. Available from: http://materials.iisc.ernet.in/~wootz/heritage/WOOTZ.htm.
[5] J Perttula, *Scandinavian Journal of Metallurgy*, 33 (2004) 92–97.
[6] OD Sherby, *ISIJ International*, 39(7) (1999) 637–648.
[7] JD Verhoeven, AH Pendray, and WE Dauksch, *JOM*, 50(9) (1998) 58–64.
[8] EM Taleff et al., *Materials Characterization*, 46 (2001) 11–18.
[9] J Perttula, *Scandinavian Journal of Metallurgy*, 30(2) (2001) 65–68.
[10] AH Pendray, *How to make a Damascus blade*, in *Scientific American*, 2001.
[11] JD Verhoeven, *Materials Technology, Steel Research*, 73(8) (2002) 356–365.
[12] J Wadsworth, *Materials Characterization*, 47 (2001) 163–165.
[13] JD Verhoeven et al., *Materials Characterization*, 30 (1993) 187–200.
[14] JD Verhoeven et al., *Materials Characterization*, 24 (1990) 205–227.
[15] MR Barnett and R Balasubramaniam, *Indian Journal of History of Science*, 42 (2007) 633–648.
[16] DT Peterson et al., *Materials Characterization*, 24 (1990) 355–374.
[17] V Kumar, *Material and Texture Characterization of Deformed Hypereutectoid (Wootz) Steel*, Indian Institute of Technology, Kanpur, 2007.
[18] A Sullivan, M Barnett, and R Balasubramaniam, *Microsc. Microanal.*, 13 (suppl 2) (2007) 1104–1105.
[19] D Jeffery, *Iron Processing*, 24 (2004) 13–16.
[20] V Randle and O Engler, *Introduction to texture analysis, macrotexture, microtexture and orientation mapping*, Gordon and Breach Science Publishers, Amsterdam, The Netherlands, 2000.
[21] HJ Bunge, *Texture Analysis in Materials Science*, Butterworths, London, 1982.
[22] JD Verhoeven and ED Gibson, *Metallurgical and Materials Transactions A*, 29A (1998) 1181–1189.
[23] RE Reed-Hill and R Abbaschian, *Physical Metallurgy Principles*. 3rd Edition, Boston, PWS-KENT Publishing Company, 1991.
[24] The authors wish to note that Professor Balasubramaniam recently passed away and want to acknowledge his contribution to this research. Without him it could not have progressed. We hope this work can continue although his involvement will be sadly missed.